Fermi Detection of a Luminous γ-ray Pulsar in a Globular Cluster

The Fermi LAT Collaboration[1,2]

[1] All authors with their affiliations appear at the end of this paper.

[2] Corresponding authors: P. C. C. Freire, pfreire@mpifr-bonn.mpg.de;
T. J. Johnson, tyrel.j.johnson@gmail.com;D. Parent, dmnparent@gmail.com;
C. Venter, Christo.Venter@nwu.ac.za.

November 17, 2011

We report the Fermi Large Area Telescope detection of γ-ray (>100 megaelectronvolts) pulsations from pulsar J1823−3021A in the globular cluster NGC 6624 with high significance ($\sim 7\,\sigma$). Its γ-ray luminosity $L_\gamma = (8.4 \pm 1.6) \times 10^{34}$ ergs per second, is the highest observed for any millisecond pulsar (MSP) to date, and it accounts for most of the cluster emission. The non-detection of the cluster in the off-pulse phase implies that its contains < 32 γ-ray MSPs, not $\sim$100 as previously estimated. The γ-ray luminosity indicates that the unusually large rate of change of its period is caused by its intrinsic spin-down. This implies that J1823−3021A has the largest magnetic field and is the youngest MSP ever detected, and that such anomalous objects might be forming at rates comparable to those of the more normal MSPs.

Since its launch in 2008, the Large Area Telescope (LAT) on board the Fermi Gamma-ray Space Telescope (*1*) has detected whole populations of objects previously unseen in the γ-ray band. These include globular clusters (GCs), which are ancient spherical groups of $\sim$

10^5 stars held together by their mutual gravity. As a class, their γ-ray spectra show evidence for an exponential cut-off at high energies (*2, 3*), a characteristic signature of magnetospheric pulsar emission. This is not surprising because radio surveys have shown that GCs contain large numbers of pulsars (*4*), neutron stars that emit radio and in some cases X-ray and γ-ray pulsations.

The first GC detected at γ-ray energies was 47 Tucanae (*5*), soon followed by Terzan 5 (*6*) and nine others (*2, 3*). Even so, no individual pulsars in these clusters were firmly identified in γ-rays (*7*). GCs are more distant than most γ-ray pulsars observed in the Galactic disk (*8*), thus most pulsars in them should be too faint to be detected individually. The Fermi LAT lacks the spatial resolution required to resolve the pulsars in GCs, which tend to congregate within the inner arcminute of the cluster. Hence, γ-ray photons emitted by all pulsars in a given GC increase the photon background in the folded γ-ray profiles of each individual pulsar in that cluster.

One of the GCs detected at γ-ray energies is NGC 6624 (*3*), located at a distance $d = 8.4 \pm 0.6\,\mathrm{kpc}$ from Earth (*9*). With a radio flux density at 400 MHz of $S_{400} = 16$ mJy (*10*), J1823$-$3021A is the brightest of the six pulsars known in the cluster. It has been regularly timed with the Jodrell Bank and Parkes radio telescopes since discovery, and with the Nançay radio telescope since the launch of the Fermi satellite. The resulting radio ephemeris (Table S1) describes the measured pulse times of arrival very well for the whole length of the Fermi mission, the root mean square of the timing residuals being 0.1% of the pulsar rotational period.

Thus we can confidently use it to assign a pulsar spin phase ϕ to every γ-ray (>0.1 GeV) photon arriving at the Fermi-LAT from the direction (within 0.8°) of the pulsar. We selected photons that occurred between 4 August 2008 and 4 October 2010 that pass the "Pass 6 diffuse" γ-ray selection cuts (*1*). The resulting pulsed γ-ray signal (above 0.1 GeV, Fig. 1) is very robust, with an H-test value of 64 (*11*) corresponding to 6.8 σ significance. The data are well modeled by a power law with spectral index 1.4 ± 0.3 and an exponential cutoff at an energy of 1.3 ± 0.6 GeV, typical of the values found for other γ-ray pulsars [see supporting online material (SOM)]. The two peaks are aligned, within uncertainties, with the two main radio components at spin phases $\phi_1 = 0.01 \pm 0.01$ and $\phi_2 = 0.64 \pm 0.01$ (Fig. 1).

The pulsed flux above 0.1 GeV, averaged over time, is $F_\gamma = (1.1 \pm 0.1 \pm 0.2) \times 10^{-11}\,\mathrm{erg\,cm^{-2}\,s^{-1}}$, where the first errors are statistical and the second are systematic (SOM). The large distance of NGC 6624 implies that J1823−3021A is one of the most distant γ-ray pulsars detected (*8*). This makes it the most luminous γ-ray MSP to date (*12*): Its total emitted power is $L_\gamma = 4\pi d^2 f_\Omega F_\gamma = (8.4 \pm 1.6 \pm 1.5) \times 10^{34}\,(f_\Omega/0.9)\,\mathrm{erg\,s^{-1}}$. We obtained the statistical uncertainty by adding the uncertainties of d and F_γ in quadrature. The term f_Ω is the power per unit surface across the whole sky divided by power per unit surface received at Earth's location; detailed modeling of the γ and radio light curves provides a best fit centered at 0.9, but with a possible range from 0.3 to 1.8 (SOM).

The LAT image of the region around NGC 6624 during the on-pulse interval ($0.60 < \phi < 0.67$ and $0.90 < \phi < 1.07$) shows a bright and isolated γ-ray source that is consistent with the location of J1823−3021A (Fig. 2); in the off-pulse region ($0.07 < \phi < 0.60$ and $0.67 < \phi < 0.90$) no point sources in the energy band 0.1 - 100 GeV are detectable. Assuming a typical pulsar spectrum with a spectral index of 1.5 and a cut-off energy of 3 GeV, we derived, after scaling to the full pulse phase, a 95% confidence level upper limit on the point source energy flux of $5.5 \times 10^{-12}\,\mathrm{erg\,cm^{-2}\,s^{-1}}$. Thus, J1823−3021A dominates the total γ-ray emission of the cluster. The combined emission of all other MSPs in the cluster plus any off-pulse emission from J1823−3021A is not detectable with present sensitivity. No other pulsars are detected in a pulsation search either.

Under the assumption that the γ-ray emission originates from NGC 6624, (*3*) estimated the total number of MSPs to be $N_{\mathrm{MSP}} = 103^{+104}_{-46}$. Assuming an average γ-ray luminosity for each

MSP (*5, 2*), similar to the approximation made by (*3*), our off-pulse flux upper limit implies that $N_{\rm MSP} < 32$. This is consistent with the estimate $N_{\rm MSP} = 30 \pm 15$ derived from the correlation between γ-ray luminosity and encounter rate (*2*). Clearly, the MSP number estimate of (*3*) is skewed by the presence of a single bright pulsar contributing disproportionately to its emission (*13*). The off-pulse emission limits can also be used to constrain alternative models for the γ-ray emission from globular clusters, like those invoking inverse Compton (IC) radiation (*14, 15*).

The spin period of J1823−3021A, 5.44 ms, is typical of MSPs. However, its rate of change $\dot{P}_{\rm obs} = +3.38 \times 10^{-18}\,{\rm s\,s^{-1}}$ is one to two orders of magnitude larger than for other MSPs with the exception of J1824−2452A, a pulsar in the GC M28 (*16*) that has a similarly large $\dot{P}_{\rm obs}$ (*17*). A possible explanation is that $\dot{P}_{\rm obs}$ is due mostly to the changing Doppler shift caused by the pulsar's acceleration in the gravitational field of the cluster along the line of sight (a_l):

$$\left(\frac{\dot{P}_{\rm obs}}{P}\right) = \left(\frac{\dot{P}}{P}\right) + \frac{a_l}{c}. \quad (1)$$

If the globular cluster has a reliable mass model, we could use it to estimate lower and upper limits for a_l and estimate upper and lower limits for $\dot{P}$ (*18*). For NGC 6624 the collapsed nature of its core precludes the derivation of a reliable mass model. Furthermore, radio timing (Table S1) shows that J1823−3021A is only $0''.4 \pm 0''.1$ (a projected distance of 0.018 ± 0.004 pc) from the center of the cluster (*19*), where the values of a_l can be largest. For this reason, it has been suggested (*10*) that J1823−3021A is a "normal" MSP (i.e., with small $\dot{P}$); its large $\dot{P}_{\rm obs}$ being due to its acceleration in the cluster. This conclusion was apparently strengthened by the detection of a second derivative of the spin period $\ddot{P} = -1.7 \times 10^{-29}\,{\rm s^{-1}}$ (*20*). This could originate in a time variation of a_l resulting from interaction with a nearby object (*21*). If sustained it would reverse the sign of $\dot{P}_{\rm obs}$ in $\sim$6000 years; suggesting again that the large $\dot{P}_{\rm obs}$ is not only due to dynamical effects, but is possibly a transient feature.

However, the total observed γ-ray emission L_γ must represent a fraction $\eta < 1$ of the available rotational energy loss, $\dot{E} = 4\pi^2 I\dot{P}/P^3$, where I is the pulsar's moment of inertia. Although I depends on the unknown mass of the pulsar and the unknown equation of state for dense matter, the standard asumption $I = 10^{45}\,\mathrm{g\,cm^2}$ is a reasonable value for a 1.4-$M_\odot$ (mass of the Sun) neutron star. This implies $\dot{P} > 3.4 \times 10^{-19}\,(f_\Omega/0.9)(I/10^{45}\mathrm{g\,cm^2})^{-1}\,\mathrm{s\,s^{-1}}$. Thus even an unrealistic γ-ray efficiency $\eta = 1$ would imply that $\dot{P}$ is already ~10% of $\dot{P}_{\rm obs}$. If we assume instead $\dot{P} \simeq \dot{P}_{\rm obs}$, then $\dot{E} = 8.3 \times 10^{35}$ erg s^{-1} and $\eta = 0.1\times(f_\Omega/0.9)(I/10^{45}\mathrm{g\,cm^2})^{-1}$. Comparison with the observed γ-ray efficiencies of other MSPs (*12, 8*) shows this to be a more reasonable range of values; $\eta \sim 0.1$ also represents the upper limit derived for the average efficiency of MSPs in 47 Tucanae (*5*). Therefore, our γ-ray detection of J1823$-$3021A indicates that it is unusually energetic and that most of $\dot{P}_{\rm obs}$ is due to its intrinsic spin-down. The pulsar has other features that suggest it is indeed unusually energetic: Its alignment of radio and γ-ray profiles has previously only been observed for the Crab pulsar (*22*) and three fast, energetic MSPs: J1939+2134 (the first MSP to be discovered), J1959+2048 (*23*) and J0034$-$0534 (*24*). Like some of these energetic pulsars and PSR J1824$-$2452A, J1823$-$3021A emits giant radio pulses (*25*) and has a high 400 MHz radio luminosity of $L_{400} \simeq 1.1$ Jy kpc^2 (*10*), the third highest among known MSPs. However the correlation between $\dot{E}$ and radio luminosity is far from perfect given the uncertainties in the distance estimates, moment of inertia, beaming effects and possibly intrinsic variations of the emission efficiencies. Finally, J1939+2134 also has a large $\ddot{P}$ (*26*), which is thought to be caused by timing noise (TN), which scales roughly with $P^{-1.1}\dot{P}$ (*27*). In the case of J1823$-$3021A, if $\dot{P} \simeq \dot{P}_{\rm obs}$, then TN should be one order of magnitude larger than for J1939+2134; instead its $\ddot{P}$ is $\sim 1.5 \times 10^2$ larger than that of J1939+2134. This is possible given the observed scatter around the TN scaling law. Thus TN might account for the $\ddot{P}$ of J1823$-$3021A, but this is far more likely if $\dot{P} \simeq \dot{P}_{\rm obs}$.

If $\dot{P} \simeq \dot{P}_{\rm obs}$, we can estimate the strength of its surface dipole magnetic field: $B_0 = 3.2 \times 10^{19}\mathrm{G}\sqrt{\dot{P}P(I/10^{45}\,\mathrm{g\,cm^2})}(R/10\,\mathrm{km})^{-3} \simeq 4.3 \times 10^9$ G (*28*) [where R is the neutron star (NS) radius, generally assumed to be 10 km]. MSPs are thought to start as normal NSs with $B_0 \sim 10^{11-13}$ G which are then spun up by the accretion of matter and angular momentum from a companion star. This process is thought to decrease their magnetic field to $B_0 \sim 10^{7-9}$ G; but the exact mechanism responsible for this is currently not well understood. Our value of B_0 shows that for J1823−3021A this decrease was not as pronounced as for other MSPs.

As accretion spins up the NS, it eventually reaches an equilibrium spin period (*29*) given by:

$$P_{\rm init} = 2.4{\rm ms}\left(\frac{B_0}{10^9{\rm G}}\right)^{6/7}\left(\frac{M}{M_\odot}\right)^{-5/7}\left(\frac{R}{10^4{\rm m}}\right)^{18/7}\left(\frac{\dot{M}}{\dot{M}_{\rm Edd}}\right)^{-3/7}, \tag{2}$$

where M is the NS mass, $\dot{M}$ is the accretion rate and $\dot{M}_{\rm Edd}$ is the maximum possible stable accretion rate for a spherical configuration (known as the Eddington rate). Beyond this, the pressure of accretion-related radiation starts preventing further accretion. After accretion ceases, the newly formed radio MSP will have $P_{\rm init}$ as its initial spin period. Assuming $\dot{M} = \dot{M}_{\rm Edd}$, $M = 1.4\,M_\odot$ and $R =$10 km (as in our estimates of B_0), we obtain $P_{\rm init} = 1.9\,{\rm ms}(B_0/10^9{\rm G})^{6/7}$. For the value of B_0 calculated above, we get $P_{\rm init} = 6.6\,$ms; that is, even if accretion had proceeded at the Eddington rate, the pulsar would not have been spun up to its present spin frequency. This is also the case for the other such “anomalous” MSP, J1824−2452A (*17*); for all others we have $P > P_{\rm init}$. A possible explanation is that for these two objects M and I do not correspond to the assumptions above. If, for example, $\eta = 0.15$, $M = 1.8\,M_\odot$ and $I = 1.8 \times 10^{45}{\rm g\,cm}^2$ (*30*) we obtain $B_0 = 3.6 \times 10^9$ G and $P_{\rm init} = 4.7\,{\rm ms}$. A second possibility, suggested by eq. 2, is super-Eddington accretion (more precisely, $\dot{M} > 1.6\,\dot{M}_{\rm Edd}$); this can happen for non-spherical mass accretion. A third possibility is that the value of B_0 was smaller during accretion (resulting in a smaller $P_{\rm init}$), and that B_0 has increased since then. This has been observed for some normal pulsars (*31*); however there is no evidence of such behavior for any other MSPs.

In any case, the conclusion that $\dot{P} \simeq \dot{P}_{\rm obs}$ implies a characteristic age $\tau_c = P/(2\dot{P}) = 25$ million years. This is likely an over-estimate of the true age of the pulsar, particularly given that $P_{\rm init}$ is likely to be similar to P. Thus J1823−3021A is likely to be the youngest MSP ever detected; only J1824−2452A might have a comparable age. Because of their large $\dot{P}$s both objects will be observable as MSPs for a time that is $\sim 10^2$ shorter than the ~ 100 "normal" radio-bright MSPs known in GCs. Statistically, this suggests that, at least in GCs, anomalous high B-field MSPs like J1823−3021A and J1824−2452A are forming at rates comparable to those of the more "normal", radio-bright MSPs.

References and Notes

1. W. B. Atwood *et al.*, *Astrophys. J.* **697**, 1071 (2009).

2. A. A. Abdo *et al.*, *Astron. & Astrophys.* **524**, A75 (2010).

3. P. H. T. Tam *et al.*, *Astrophys. J.* **729**, 90 (2011).

4. See updated list of pulsars in globular clusters and references in http://www.naic.edu/∼pfreire/GCpsr.html.

5. A. A. Abdo *et al.*, *Science* **325**, 845 (2009).

6. A. K. H. Kong *et al.* *Astrophys. J.* **712**, L36 (2010).

7. The AGILE collaboration reported a low-significance detection of the MSP J1824−2452A in the globular cluster M28 that has not been confirmed (*32*).

8. A. A. Abdo *et al.*, *Astrophys. J. Supp.* **187**, 460 (2010).

9. E. Valenti, F. R. Ferraro, L. Origlia, *Astron. J.* **133**, 1287 (2007).

10. J. D. Biggs *et al.*, *Mon. Not. R. Astron. Soc.* **267**, 125 (1994).

11. O. C. de Jager, I. Büsching, *Astron. & Astrophys.* **517**, L9 (2010).

12. A. A. Abdo *et al.* (Fermi-LAT collaboration), *Science* **325**, 848 (2009).

13. A. S. Fruchter & W. M. Goss, *Astrophys. J.***536**, 865 (2000).

14. W. Bednarek, J. Sitarek, *Mon. Not. R. Astron. Soc.* **377**, 920 (2007).

15. K. S. Cheng *et al.* *Astrophys. J.* **723**, 1219 (2010).

16. A. G. Lyne *et al.*, *Nature* **328**, 399 (1987).

17. R. S. Foster *et al.* *Astrophys. J.* **326**, L13 (1988).

18. P. C. Freire, *et al.*, *Mon. Not. R. Astron. Soc.* **340**, 1359 (2003).

19. R. Goldsbury, *et al.*, *Astron. J.* **140**, 1830 (2010).

20. G. Hobbs *et al.* *Mon. Not. R. Astron. Soc.* **353**, 1311 (2004).

21. E. S. Phinney, *Royal Society of London Philosophical Transactions Series A* **341**, 39 (1992).

22. A. A. Abdo, *et al.*, *Astrophys. J.* **708**, 1254 (2010).

23. L. Guillemot, *et al.*, arXiv:1101.0669 (2011).

24. A. A. Abdo, *et al.*, *Astrophys. J.* **712**, 957 (2010).

25. H. S. Knight, *Mon. Not. R. Astron. Soc.* **378**, 723 (2007).

26. Cognard, I., Bourgois, G., Lestrade, J.-F., et al. 1995, *Astron. & Astrophys.* **296**, 169 (1995)

27. Shannon, R. M., & Cordes, J. M., *Astrophys. J.* **725**, 1607 (2010).

28. Lorimer, D. R., & Kramer, M. Handbook of pulsar astronomy, by D. R. Lorimer and M. Kramer. Cambridge observing handbooks for research astronomers, Vol. 4. Cambridge, UK: Cambridge University Press (2004).

29. M. A. Alpar, A. F. Cheng, M. A. Ruderman, & J. Shaham, *Nature* **300**, 728 (1982).

30. Worley, A., Krastev, P. G., & Li, B.-A., *Astrophys. J.* **685**, 390 (2008)

31. C. Espinoza *et al.* arXiv:1109.2740 (2011).

32. A. Pellizzoni *et al.*, *Astrophys. J.* **695**, L115 (2009)

33. D. A. Smith, *et al.*, *Astron. & Astrophys.* **492**, 923 (2008).

34. G. Hobbs *et al.* *Mon. Not. R. Astron. Soc.* **353**, 1311 (2004).

35. I. Cognard, G. Theureau, G. Desvignes, R. Ferdman, arXiv:0911.1612 (2009).

36. G. B. Hobbs, *et al.*, *Mon. Not. R. Astron. Soc.* **369**, 655 (2006).

37. W. B. Atwood, *et al.* (Fermi-LAT collaboration), *Astrophys. J.* **697**, 1071 (2009).

38. P. S. Ray, M. Kerr, D. Parent *et al.*, *Astrophys. J. Supp.* **194**, 17 (2011).

39. A. A. Abdo, *et al.* (Fermi-LAT collaboration), *Astrophys. J. Supp.* **188**, 405 (2010).

40. A. A. Abdo, *et al.* (Fermi-LAT collaboration), *Astrophys. J. Supp.* **187**, 460 (2010).

41. A. A. Abdo, *et al.* (Fermi-LAT collaboration), *Astron. & Astrophys.* **524**, A75 (2010).

42. P. H. T. Tam *et al.*, *Astrophys. J.* **729**, 90 (2011).

43. J. K. Daugherty, A. K. Harding, *Astrophys. J.* **252**, 337 (1982).

44. J. K. Daugherty, A. K. Harding, *Astrophys. J.* **458**, 278 (1996).

45. K. S. Cheng, C. Ho, M. Ruderman, *Astrophys. J.* **300**, 500 (1986a).

46. K. S. Cheng, C. Ho, M. Ruderman, *Astrophys. J.* **300**, 522 (1986b).

47. R. W. Romani, *Astrophys. J.* **470**, 469 (1996).

48. J. Arons, *Astrophys. J.* **266**, 215 (1983).

49. J. Dyks, B. Rudak, *Astrophys. J.* **598**, 1201 (2003).

50. M. Morini, *Mon. Not. R. Astron. Soc.* **202**, 495 (1983).

51. K. P. Watters, R. W. Romani, *et al. Astrophys. J.* **695**, 1289 (2009).

52. C. Venter, A. K. Harding, & L. Guillemot, *Astrophys. J.* **707**, 800 (2009).

53. A. A. Abdo *et al.* (Fermi-LAT collaboration), *Astrophys. J.* **712**, 957 (2010).

54. I. H. Stairs, S. E. Thorsett, & F. Camilo, *Astrophys. J. Supp.* **123**, 627 (1999).

55. T. J. Johnson, Ph. D. Thesis, University of Maryland, College Park, U.S.A. (2011).

The Fermi-LAT Collaboration acknowledges support from a number of agencies and institutes for both development and the operation of the LAT as well as scientific data analysis. These include NASA and the Department of Energy in the United States; Comissariat à l'Energie Atomique et aux Énergies Alternatives / Institut de Recherche sur les Lois Fundamentales de l'Universe (CEA/IRFU) and Institut National de Physique Nucléaire et de Physique des Particules, Centre National de la Recherche Scientifique (IN2P3/CNRS) in France; Agenzia Spaziale Italiana (ASI) and Instituto Nazionale di Fisica Nucleare (INFN) in Italy; Ministry of Education, Culture, Sports, Science and Technology (MEXT), Energy Accelerator Research Organization (KEK), and Japan Aerospace Exploration Agency (JAXA) in Japan; and the K. A. Wallenberg Foundation, Swedish Research Council and the National Space Board in

Sweden. Additional support from Instituto Nazionale di Astrofisica (INAF) in Italy and Centre National d'Etudes Spaciales (CNES) in France for science analysis during the operations phase is also gratefully acknowledged. The Nançay Radio Observatory is operated by the Paris Observatory, associated with the CNRS. The Lovell Telescope is owned and operated by the University of Manchester as part of the Jodrell Bank Centre for Astrophysics with support from the Science and Technology Facilities Council of the United Kingdom. Fermi LAT data, γ-ray diffuse models, and radio pulsar ephemeris are available from the Fermi Science Support Center (http://fermi.gsfc.nasa.gov/ssc/data/access). We also thank the anonymous referees and the Science editors for the very constructive suggestions.

The Fermi LAT Collaboration: P. C. C. Freire[1], A. A. Abdo[2], M. Ajello[3], A. Allafort[3], J. Ballet[4], G. Barbiellini[5,6], D. Bastieri[7,8], K. Bechtol[3], R. Bellazzini[9], R. D. Blandford[3], E. D. Bloom[3], E. Bonamente[10,11], A. W. Borgland[3], M. Brigida[12,13], P. Bruel[14], R. Buehler[3], S. Buson[7,8], G. A. Caliandro[15], R. A. Cameron[3], F. Camilo[16], P. A. Caraveo[17], C. Cecchi[10,11], Ö. Çelik[18,19,20], E. Charles[3], A. Chekhtman[21], C. C. Cheung[22], J. Chiang[3], S. Ciprini[23,11], R. Claus[3], I. Cognard[24], J. Cohen-Tanugi[25], L. R. Cominsky[26], F. de Palma[12,13], C. D. Dermer[27], E. do Couto e Silva[3], M. Dormody[28], P. S. Drell[3], R. Dubois[3], D. Dumora[29], C. M. Espinoza[30], C. Favuzzi[12,13], S. J. Fegan[14], E. C. Ferrara[18], W. B. Focke[3], P. Fortin[14], Y. Fukazawa[31], P. Fusco[12,13], F. Gargano[13], D. Gasparrini[32], N. Gehrels[18], S. Germani[10,11], N. Giglietto[12,13], F. Giordano[12,13], M. Giroletti[33], T. Glanzman[3], G. Godfrey[3], I. A. Grenier[4], M.-H. Grondin[34,35], J. E. Grove[27], L. Guillemot[1], S. Guiriec[36], D. Hadasch[15], A. K. Harding[18], G. Jóhannesson[37], A. S. Johnson[3], T. J. Johnson[18,22,46,2], S. Johnston[38], H. Katagiri[39], J. Kataoka[40], M. Keith[38], M. Kerr[3], J. Knödlseder[41,3], M. Kramer[30,1], M. Kuss[9], J. Lande[3], L. Latronico[43], S.-H. Lee[44], M. Lemoine-Goumard[29,45], F. Longo[5,6], F. Loparco[12,13], M. N. Lovellette[27], P. Lubrano[10,11], A. G. Lyne[30], R. N. Manchester[38], M. Marelli[17], M. N. Mazziotta[13], J. E. McEnery[18,46], P. F. Michelson[3], T. Mizuno[31], A. A. Moiseev[19,46], C. Monte[12,13], M. E. Monzani[3], A. Morselli[47], I. V. Moskalenko[3], S. Murgia[3], T. Nakamori[40],

P. L. Nolan[3], J. P. Norris[48], E. Nuss[25], T. Ohsugi[49], A. Okumura[3,50], N. Omodei[3], E. Orlando[3,51], M. Ozaki[50], D. Paneque[52,3], D. Parent[2], M. Pesce-Rollins[9], M. Pierbattista[4], F. Piron[25], T. A. Porter[3], S. Rainò[12,13], S. M. Ransom[53], P. S. Ray[27], A. Reimer[54,3], O. Reimer[54,3], T. Reposeur[29], S. Ritz[28], R. W. Romani[3], M. Roth[55], H. F.-W. Sadrozinski[28], P. M. Saz Parkinson[28], C. Sgrò[9], R. Shannon[38], E. J. Siskind[56], D. A. Smith[29], P. D. Smith[57], P. Spinelli[12,13], B. W. Stappers[30], D. J. Suson[58], H. Takahashi[49], T. Tanaka[3], T. M. Tauris[59,1], J. B. Thayer[3], G. Theureau[24], D. J. Thompson[18], S. E. Thorsett[60], L. Tibaldo[7,8], D. F. Torres[15,61], G. Tosti[10,11], E. Troja[18,62], J. Vandenbroucke[3], A. Van Etten[3], V. Vasileiou[25], C. Venter[63], G. Vianello[3,64], N. Vilchez[41,42], V. Vitale[47,65], A. P. Waite[3], P. Wang[3], K. S. Wood[27], Z. Yang[66,67], M. Ziegler[28], S. Zimmer[66,67]

[1] Max-Planck-Institut für Radioastronomie, Auf dem Hügel 69, 53121 Bonn, Germany. [2] Center for Earth Observing and Space Research, College of Science, George Mason University, Fairfax, VA 22030, resident at Naval Research Laboratory, Washington, DC 20375, USA. [3] W. W. Hansen Experimental Physics Laboratory, Kavli Institute for Particle Astrophysics and Cosmology, Department of Physics and SLAC National Accelerator Laboratory, Stanford University, Stanford, CA 94305, USA. [4] Laboratoire AIM, CEA-IRFU/CNRS/Université Paris Diderot, Service d'Astrophysique, CEA Saclay, 91191 Gif sur Yvette, France. [5] Istituto Nazionale di Fisica Nucleare, Sezione di Trieste, I-34127 Trieste, Italy. [6] Dipartimento di Fisica, Università di Trieste, I-34127 Trieste, Italy. [7] Istituto Nazionale di Fisica Nucleare, Sezione di Padova, I-35131 Padova, Italy. [8] Dipartimento di Fisica "G. Galilei", Università di Padova, I-35131 Padova, Italy. [9] Istituto Nazionale di Fisica Nucleare, Sezione di Pisa, I-56127 Pisa, Italy. [10] Istituto Nazionale di Fisica Nucleare, Sezione di Perugia, I-06123 Perugia, Italy. [11] Dipartimento di Fisica, Università degli Studi di Perugia, I-06123 Perugia, Italy. [12] Dipartimento di Fisica "M. Merlin" dell'Università e del Politecnico di Bari, I-70126 Bari, Italy. [13] Istituto Nazionale di Fisica Nucleare, Sezione di Bari, 70126 Bari, Italy. [14] Labora-

toire Leprince-Ringuet, École polytechnique, CNRS/IN2P3, Palaiseau, France. [15] Institut de Ciències de l'Espai (IEEE-CSIC), Campus UAB, 08193 Barcelona, Spain. [16] Columbia Astrophysics Laboratory, Columbia University, New York, NY 10027, USA. [17] INAF-Istituto di Astrofisica Spaziale e Fisica Cosmica, I-20133 Milano, Italy. [18] NASA Goddard Space Flight Center, Greenbelt, MD 20771, USA. [19] Center for Research and Exploration in Space Science and Technology (CRESST) and NASA Goddard Space Flight Center, Greenbelt, MD 20771, USA. [20] Department of Physics and Center for Space Sciences and Technology, University of Maryland Baltimore County, Baltimore, MD 21250, USA. [21] Artep Inc., 2922 Excelsior Springs Court, Ellicott City, MD 21042, resident at Naval Research Laboratory, Washington, DC 20375, USA. [22] National Research Council Research Associate, National Academy of Sciences, Washington, DC 20001, resident at Naval Research Laboratory, Washington, DC 20375, USA. [23] ASI Science Data Center, I-00044 Frascati (Roma), Italy. [24] Laboratoire de Physique et Chimie de l'Environnement, LPCE UMR 6115 CNRS, F-45071 Orléans Cedex 02, and Station de radioastronomie de Nançay, Observatoire de Paris, CNRS/INSU, F-18330 Nançay, France. [25] Laboratoire Univers et Particules de Montpellier, Université Montpellier 2, CNRS/IN2P3, Montpellier, France. [26] Department of Physics and Astronomy, Sonoma State University, Rohnert Park, CA 94928-3609, USA. [27] Space Science Division, Naval Research Laboratory, Washington, DC 20375-5352, USA. [28] Santa Cruz Institute for Particle Physics, Department of Physics and Department of Astronomy and Astrophysics, University of California at Santa Cruz, Santa Cruz, CA 95064, USA. [29] Université Bordeaux 1, CNRS/IN2p3, Centre d'Études Nucléaires de Bordeaux Gradignan, 33175 Gradignan, France. [30] Jodrell Bank Centre for Astrophysics, School of Physics and Astronomy, The University of Manchester, M13 9PL, UK. [31] Department of Physical Sciences, Hiroshima University, Higashi-Hiroshima, Hiroshima 739-8526, Japan. [32] Agenzia Spaziale Italiana (ASI) Science Data Center, I-00044 Frascati (Roma), Italy. [33] INAF Istituto di Radioastronomia, 40129 Bologna, Italy. [34] Max-

Planck-Institut für Kernphysik, D-69029 Heidelberg, Germany. [35] Landessternwarte, Universität Heidelberg, Königstuhl, D 69117 Heidelberg, Germany. [36] Center for Space Plasma and Aeronomic Research (CSPAR), University of Alabama in Huntsville, Huntsville, AL 35899, USA. [37] Science Institute, University of Iceland, IS-107 Reykjavik, Iceland. [38] CSIRO Astronomy and Space Science, Australia Telescope National Facility, Epping NSW 1710, Australia. [39] College of Science, Ibaraki University, 2-1-1, Bunkyo, Mito 310-8512, Japan. [40] Research Institute for Science and Engineering, Waseda University, 3-4-1, Okubo, Shinjuku, Tokyo 169-8555, Japan. [41] CNRS, IRAP, F-31028 Toulouse cedex 4, France. [42] GAHEC, Université de Toulouse, UPS-OMP, IRAP, Toulouse, France. [43] Istituto Nazionale di Fisica Nucleare, Sezioine di Torino, I-10125 Torino, Italy. [44] Yukawa Institute for Theoretical Physics, Kyoto University, Kitashirakawa Oiwake-cho, Sakyo-ku, Kyoto 606-8502, Japan. [45] Funded by contract ERC-StG-259391 from the European Community. [46] Department of Physics and Department of Astronomy, University of Maryland, College Park, MD 20742, USA. [47] Istituto Nazionale di Fisica Nucleare, Sezione di Roma “Tor Vergata”, I-00133 Roma, Italy. [48] Department of Physics, Boise State University, Boise, ID 83725, USA. [49] Hiroshima Astrophysical Science Center, Hiroshima University, Higashi-Hiroshima, Hiroshima 739-8526, Japan. [50] Institute of Space and Astronautical Science, JAXA, 3-1-1 Yoshinodai, Chuo-ku, Sagamihara, Kanagawa 252-5210, Japan. [51] Max-Planck Institut für extraterrestrische Physik, 85748 Garching, Germany. [52] Max-Planck-Institut für Physik, D-80805 München, Germany. [53] National Radio Astronomy Observatory (NRAO), Charlottesville, VA 22903, USA. [54] Institut für Astro- und Teilchenphysik and Institut für Theoretische Physik, Leopold-Franzens-Universität Innsbruck, A-6020 Innsbruck, Austria. [55] Department of Physics, University of Washington, Seattle, WA 98195-1560, USA. [56] NYCB Real-Time Computing Inc., Lattingtown, NY 11560-1025, USA. [57] Department of Physics, Center for Cosmology and Astro-Particle Physics, The Ohio State University, Columbus, OH 43210, USA. [59] Department of Chemistry and Physics, Purdue University Calumet, Hammond, IN 46323-2094, USA. [59] Argelander-Institut für Astronomie, Universität Bonn, 53121 Bonn, Germany. [60] Department of Physics, Willamette University, Salem, OR 97031, USA. [61] Institució Catalana de Recerca i Estudis Avançats (ICREA), Barcelona, Spain. [62] NASA Postdoctoral Program Fellow, USA. [63] Centre for Space Research, North-West University, Potchefstroom Campus, Private Bag X6001, 2520 Potchefstroom, South Africa. [64] Consorzio Interuniversitario per la Fisica Spaziale (CIFS), I-10133 Torino, Italy. [65] Dipartimento di Fisica, Università di Roma "Tor Vergata", I-00133 Roma, Italy. [66] Department of Physics, Stockholm University, AlbaNova, SE-106 91 Stockholm, Sweden. [67] The Oskar Klein Centre for Cosmoparticle Physics, AlbaNova, SE-106 91 Stockholm, Sweden.

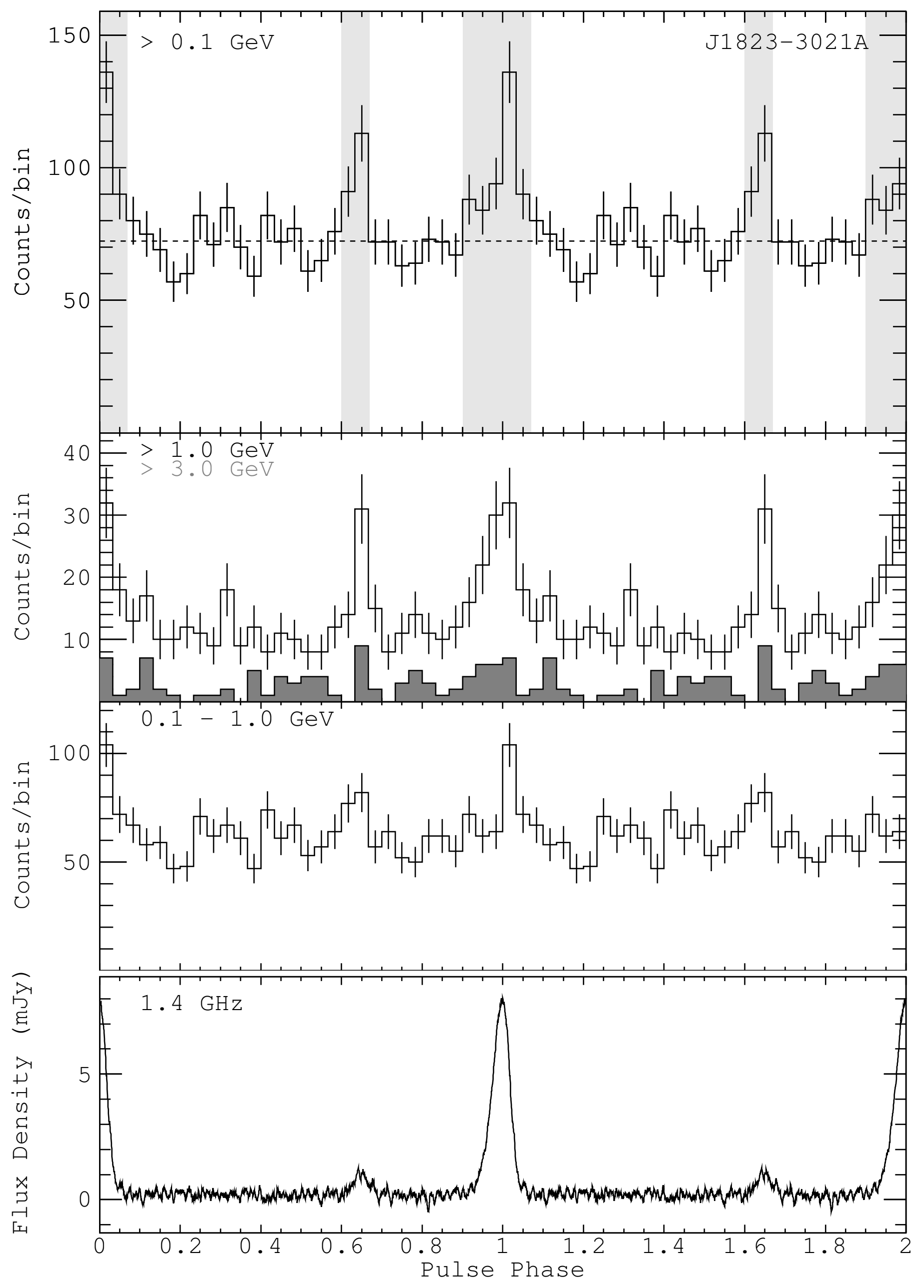

Figure 1: Phase-aligned radio and γ-ray profiles for J1823−3021A. (Bottom) Nançay 1.4 GHz radio profile. (Top and middle) γ-ray profiles obtained with the Fermi-LAT in different energy bands. The dark histogram is for events with $E > 3.0$GeV. The γ-ray background for the 0.1 GeV light curve was estimated from a surrounding ring, and it is indicated by the dashed horizontal line in the top panel. The highlighted area there shows the on-pulse region selection.

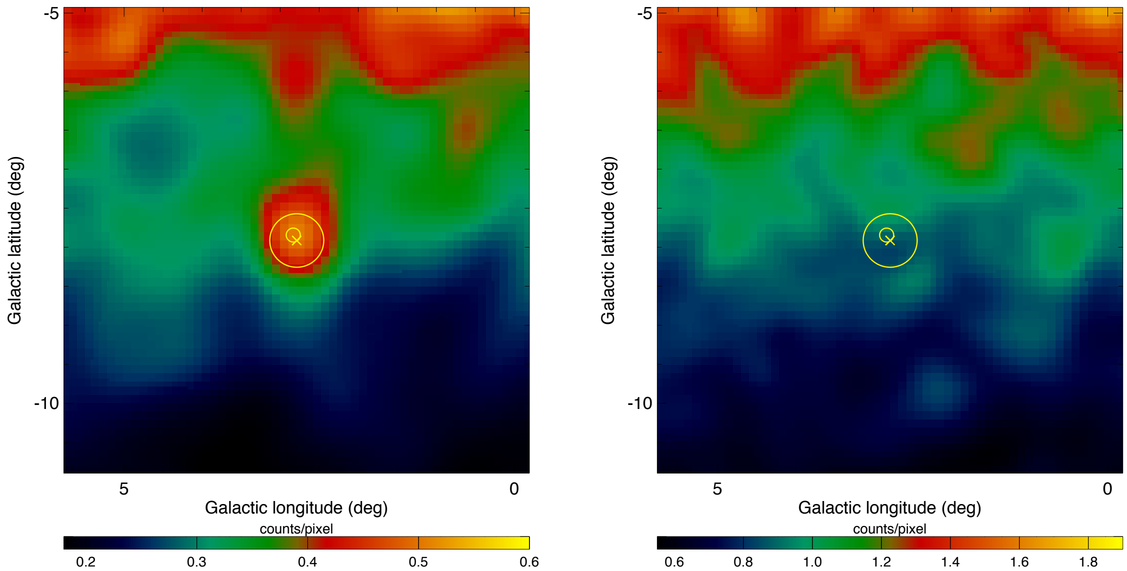

Figure 2: Fermi LAT γ-ray count map above 100 MeV for J1823−3021A during the on-pulse (Left) and off-pulse (Right) regions, as defined in Fig. 1. The $6°$ by $6°$ region is centered on the pulsar position (cross). The map was adaptively smoothed by imposing minimum signal-to-noises ratios of 13 and 16 for the on- and off-pulse regions, respectively. The large circle indicates the tidal radius of NGC 6624. The small circle shows the 99% confidence region for the location of the γ-ray source.

Supporting Online Material

Observations and data analysis

Radio Timing analysis

With the express purpose of supporting the Fermi mission (*33*), J1823−3021A is observed approximately 3 times per month with the 76-m Lovell telescope (*34*), using a 64 MHz band centered at 1404 MHz connected to an analog filterbank. Since mid-2009 observations have also been performed using a digital filterbank backend with 1024×0.5 MHz channels of which approximately 250 MHz is used. Highly precise timing measurements are also conducted with the Nançay radio telescope (*35*). These have included regular observations of J1823−3021A since mid-2006. Approximately every two months, the pulsar is observed for 1 hour at 1.4 GHz. A 128 MHz bandwidth is coherently dedispersed using powerful GPUs (Graphics Processing Units). A total of 104 pulse times of arrival (TOAs) were obtained from the two telescopes between mid-2006 and mid-2010. The TEMPO2 timing package (*36*) was used to build the timing solution, which includes the pulsar rotation frequency and its derivatives, the dispersion measure, and the pulsar position. The post-fit residuals are characterized by a weighted rms of 7.3 μs. The resulting parameters are summarized in Table S1. No trends are noticeable in the post-fit residuals.

Fermi LAT data analysis

We have observed J1823−3021A with the Large Area Telescope aboard Fermi from 2008 August 4, when the satellite began scanning-mode operations, to the end of the validity range of the pulsar radio ephemeris (2010 October 14). The data analysis presented in this paper has been performed using the LAT Science Tools package 09-21-00 and the P6 V3 Diffuse instrument response functions (IRFs). Events tagged "Pass 6 diffuse" having the highest probability of being γ-ray photons (*37*) and coming from zenith angles $< 100°$ (to reject atmospheric γ-rays from the Earth's limb) were used. Additionally, a rotational phase was assigned to each selected LAT event using the radio ephemeris as an input to the Fermi plugin (*38*) distributed with the TEMPO2 pulsar timing software.

Using the `pyLikelihood` likelihood fitting tool with the NewMinuit optimizer, we performed a binned spectral analysis to determine the energy flux and the spectral shape of the source. Events in the range 0.1–100 GeV were extracted from a 20° × 20° square region of interest (ROI) centered on the pulsar position. To reduce the effect of the Earth's atmospheric emission, the time intervals when the Earth was appreciably within the field of view (specifically, when the center of the field of view was more than 52° from the zenith) were excluded from this analysis. The Galactic diffuse emission was modeled using the *gll_iem_v02* map cube, while the extragalactic emission and residual instrument backgrounds were modeled jointly by the isotropic component *isotropic_iem_v02*. These two models are available from the Fermi Science Support Center[1]. In addition, all the sources found in an internal catalog based on 18 months of data (similar to (*39*)) above the background with significances $> 5\sigma$ and within $20°$ from the pulsar were included in the model. Sources were modeled with a power law spectrum, except for pulsars for which a power law with an exponential cut-off was used (*40*). Sources more than 5° from the pulsar were assigned fixed spectra taken from the source catalog. Spectral parameters for sources within 5° of the pulsar were left free for the analysis.

The pulsar location at the core of NGC 6624 is located just outside the 99% statistical error contour of the γ-ray source 1FGL J1823.4−3009 (*39*), based on an analysis of the first 11 months of the LAT survey data. Therefore, (*41*) did not establish an association between 1FGL J1823.4−3009 and the globular cluster. (*42*), using a larger dataset, showed that the γ-ray position lies within the (20.55′) tidal radius of the cluster. To check the association,

[1] http://fermi.gsfc.nasa.gov/ssc/data/access/lat/BackgroundModels.html

we first reevaluated the position of the γ-ray source 1FGL J1823.4$-$3009, using the on-pulse ($0.60 < \phi < 0.67$ and $0.90 < \phi < 0.07$) segment of the pulsar rotational phase (to improve the signal-to-noise ratio), to be ($\alpha_{2000} = 275.87\,^\circ$, $\delta_{2000} = -30.29\,^\circ$) with a 99% confidence error radius of 0.09$\,^\circ$. This places the pulsar radio position just inside the 99% error contour of the γ-ray source. We also investigated the off-pulse window and detected a $\sim 4\,\sigma$ point source which coincides with the position of the radio source NVSS J182324$-$300311 ($\alpha_{2000} = 275.8515\,^\circ$, $\delta_{2000} = -30.053278\,^\circ$). The signal, only observed during the first year of the Fermi mission, is located 0.11$\,^\circ$ away from the position of 1FGL J1823.4$-$3009 and 0.31$\,^\circ$ away from NGC 6624. It is likely that 1FGL J1823.4$-$3009, located between NVSS J182324$-$300311 and NGC 6624, includes contributions from both of these sources. Using the second year of data, when the nearby faint source is off, we localize the γ-ray source corresponding to the pulsar to ($\alpha_{2000} = 275.93\,^\circ$, $\delta_{2000} = -30.34\,^\circ$) with a 68% error counter radius of 0.07$\,^\circ$. This position is consistent with the radio pulsar position. We then fitted the spectrum of the pulsar at the radio pulsar position using a power law with an exponential cut-off. Figure S1 shows both the fit between 0.1 and 30 GeV (solid lines) and the spectral points derived from likelihood fits to each individual energy band in which it was assumed the pulsar had a power-law spectrum.

Light Curve Modeling

There have been two major contenders for modeling the high-energy (HE) radiation (roughly 100 MeV to 10 GeV range) from pulsars, those which assume that the observed γ-rays are emitted near the stellar surface (*43, 44*) above the magnetic polar cap and those which assume the γ-rays originate primarily in the outer magnetosphere near the light cylinder (the distance from the rotation axis $\vec{\Omega}$ at which the co-rotation equals the speed of light). Both classes of models assume that the HE γ-rays are curvature radiation from highly-relativistic electrons/positrons in the radiation-reaction regime. The two most common outer-magnetospheric emission models are the outer gap (OG; (*45, 46, 47*)) and the slot gap (*48*) models. For our purposes we took the two-pole caustic (TPC; (*49*)) model to be a geometric realization of the slot gap. TPC and OG models both assume that the emitting electrons are accelerated up to high altitudes in narrow gaps along the last-open field lines. The OG model only allows acceleration above the null-charge surface (NCS; where $\vec{\Omega} \cdot \vec{B} = 0$) whereas in the TPC model electrons are accelerated from the stellar surface. The HE pulse profiles in these outer-magnetospheric models are the result of the accumulation of photons in narrow phase bands due to a combination of three effects: aberration (change of photon direction due to the high corotation velocity), time-of-flight delays (photons produced at higher altitudes will reach an observer earlier than those coming from lower altitudes), as well as the magnetic field line curvature (photons are assumed to be created tangential to the local magnetic field line in the corotating frame, and their direction is therefore very sensitive to the magnetic field geometry). This is referred to as caustic emission (*50*).

TPC and OG models are generally used in conjunction with a low-altitude radio cone beam geometry (e.g., (*51, 52*)). Due to the difference in altitude of the radio and γ-ray emission, there will be a phase lag between the radio and γ-ray profiles. Polar-cap (e.g., (*44*)) γ-ray emission models do predict much smaller phase lags but, due to the large open field line region of MSPs, they cannot produce the narrow peaks observed in the γ-ray light curve of PSR J1823$-$3021A. The phase-alignment of PSR J1823$-$3021A's radio and γ-ray light curves argues for overlapping γ-ray and radio emission regions. To reproduce the phase-aligned light curves we used altitude-limited versions of the TPC and OG models (alTPC and alOG, respectively) which were first introduced to model the light curves of the MSP PSR J0034$-$0534 (*53*). These are very similar to the standard TPC and OG models, except that the minimum and maximum radii of the radio emission region as well as the maximum radius of the γ-ray emission region are free parameters (the minimum γ-ray emission radius being set by the standard models). Therefore, both radio and γ-ray photons originate in a TPC or OG-like structure, with a significant amount of overlap between the two emitting regions leading to phase-aligned profiles. This implies that the radio emission is also caustic in nature, supported by polarimetric observations which find 0% linear polarization for PSR J1823−3021A (*54*). Conversely, these models provide a framework to constrain the respective radio and γ-ray emission geometries when comparing the model light curves to the data.

We have simulated γ-ray and radio light curves using alTPC and alOG models with a spin period P = 1.5 ms, steps of 1° in magnetic inclination angle (α) and viewing angle (ζ), 0.05 in accelerating emission layer width (w, normalized to the opening angle of the polar cap), and 0.10 (in units of $R_{\rm LC} = cP/(2\pi)$) for the emission altitudes. The spin period used in the simulation is less than that of PSR J1823−3021A (5.44 ms) but this quantity enters the simulation mainly through the size of the polar cap. Using models with a shorter period will, at most, overestimate any predicted off-pulse region. We have developed a Markov chain Monte Carlo (MCMC) maximum likelihood technique to jointly fit the γ-ray and radio profiles and pick the best-fit paramters (*55*). We fit the $\geq$ 500 MeV γ-ray light curve in 60 bins and rebinned the radio profile to 60 bins. For the γ-ray models the minimum emission altitudes (R^{γ}_{min}) were specified as described previously while the maximum emission altitudes were allowed to be free under the constraint $R^{\gamma}_{max} \geq 0.7\ R_{\rm LC}$. The radio emission altitudes are unconstrained save that $R^{\rm R}_{max} > R^{\rm R}_{min}$. The best-fit parameters for both models are given in Table S2; the likelihood does not prefer one model over another. The alTPC model has best-fit gap widths of 0.0. This is unphysical and should be taken to indicate that the true gap widths are between 0.0 and 0.05. Following (*52*) we can estimate the beaming factor (f_Ω) for both models using Eq. 4 of (*51*), see Table S2. Presently we are unable to provide reliable uncertainty estimates for our model predictions and, thus, can not propagate any uncertainty on f_Ω into the uncertainty on L_γ. However, while PSR J1823−3021A stands out in some respects, the shape of the observed HE light curve is very typical of known γ-ray MSPs. The best-fit geometries of (*55*) to these

MSPs yield values of f_Ω from approximately 0.3 to 1.8, with mean of 0.81 and rms of 0.36. We therefore expect the f_Ω value for J1823$-$3021A to be similar to the geometries which, in these models, produce "typical" γ-ray light curves. The high and low tails of this distribution suggest that the γ-ray efficiency could reasonably be anywhere from 3 to 20% but neither extreme affects the conclusion of the main text that most of the observed $\dot{P}$ is intrinsic to the pulsar.

Timing parameters	
Right Ascension, α (J2000)	$18^{\mathrm{h}}\ 23^{\mathrm{m}}\ 40\overset{\mathrm{s}}{.}48466(4)$
Declination, δ (J2000)	$-30^{\circ}\ 21'\ 39\overset{''}{.}988(4)$
Solar System Ephemeris	DE 405
Reference time scale	TDB
Reference time (MJD)	54939
Spin Frequency, ν (Hz)	183.823389814514(7)
First derivative of ν, $\dot{\nu}$ (10^{-15} Hz s^{-1}) ..	$-114.1351(4)$
Second derivative of ν, $\ddot{\nu}$ (10^{-25} Hz s^{-2})	5.8(1)
Dispersion Measure, DM (cm^{-3} pc)	86.864(9)
Validity Range (MJD)	53773.35 – 55483.67
RMS Timing Residuals (μs)	7.3

Table S1. Timing parameters for J1823−3021A. The center of the globular cluster is located at $\alpha = 18^{\mathrm{h}}23^{\mathrm{m}}40\overset{\mathrm{s}}{.}51 \pm 0\overset{\mathrm{s}}{.}008$, $\delta = -30^{\circ}21'39\overset{''}{.}7 \pm 0\overset{''}{.}1$.

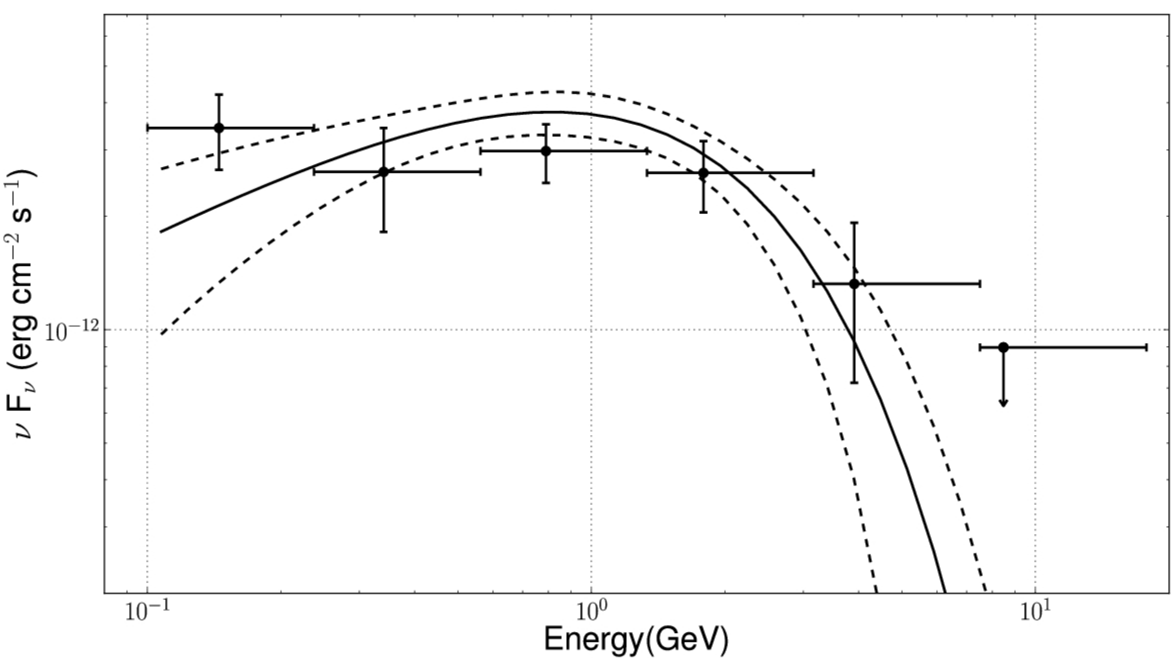

Fig. S1. γ-ray spectral energy distribution of J1823−3021A obtained with the Fermi Large Area Telescope. The solid black line shows the maximum likelihood fit to a power law with exponential cut-off. The dashed lines are $\pm 1\sigma$ uncertainties on the fit parameters. Plotted points are from likelihood fits to individual energy bands with $> 3\sigma$ detection above background for two degrees of freedom, otherwise a 95% confidence level upper limit arrow is shown. The errors are statistical only.

Best-fit Light Curve Parameters

Model	-log(Like)	f_Ω	α (°)	ζ (°)	Φ	w_γ	$w_{\rm R}$	R^γ_{max}	$R^{\rm R}_{min}$	$R^{\rm R}_{max}$
alTPC	173.8	0.9	51	68	0.017	0.00	0.00	1.0	0.2	0.9
alOG	173.6	0.9	69	68	0.017	0.05	0.10	1.2	$max\{R_{\rm NCS}, 0.2\}$	0.8

Table S2. Results of MCMC maximum likelihood fits to the γ-ray and radio light curves of PSR J1823−3021A using the alTPC and alOG models.

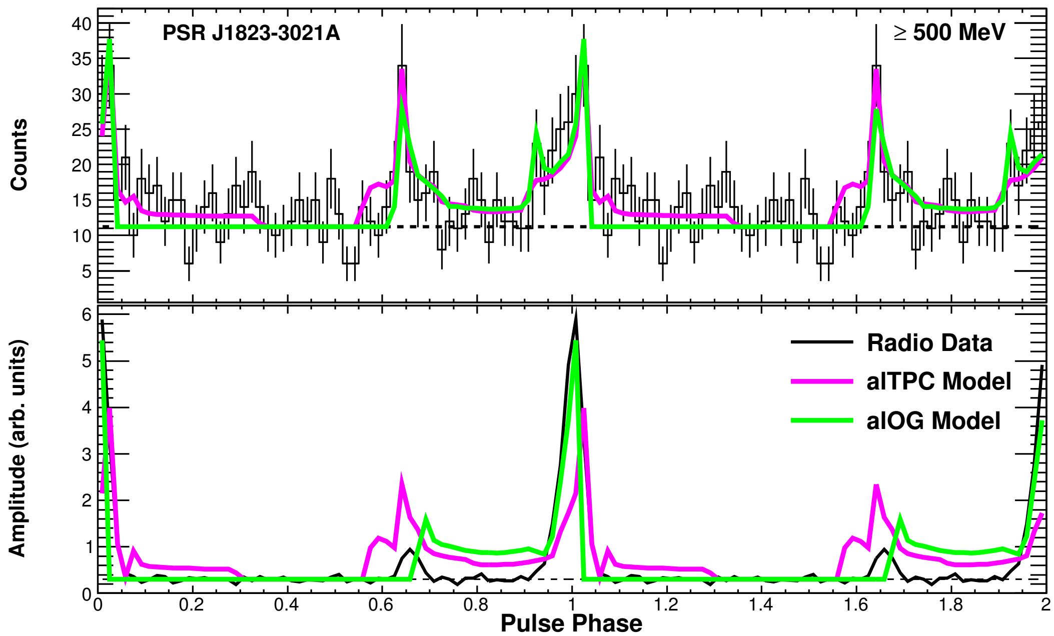

Fig. S2. Observed and best-fit γ-ray (top) and radio (bottom) light curves for PSR J1823−3021A using the alTPC (pink) and alOG (green) models described in the text. The dashed, horizontal lines in both panels correspond to the estimated background levels. The γ-ray background was estimated using an annular ring centered on the radio position with inner and outer radii of 1° and 2°, respectively. The radio background was estimated by fitting the region between 0.1 and 0.6 in phase to a constant value. The parameters of the best-fit light curves are given in Table S2.